ARTICLE NO. 79-4145

Laminar and Turbulent Flows over a Spherically Blunted Cone with Massive Surface Blowing

Ajay Kumar*
Old Dominion University, Norfolk, Va.
R. A. Graves Jr.†
NASA Langley Research Center, Hampton, Va.
and
S. N. Tiwari‡
Old Dominion University, Norfolk, Va.

Numerical solutions are presented for the flow over a spherically blunted cone with massive surface blowing. Time-dependent viscous shock layer equations are used to describe the flowfield. The boundary conditions on the body surface include a prescribed blowing rate distribution. The governing equations are solved by a time-asymptotic finite-difference method. Results presented here are only for a perfect gas-type flow at zero angle of attack. Both laminar and turbulent flow solutions are obtained. It is found that the surface blowing smooths out the effect of the curvature discontinuity at the sphere-cone juncture point on the laminar flowfield and results in a negative pressure gradient over the body. The shock slope increases on the downstream portion of the body as the surface blowing rate is increased. The turbulent flow with surface blowing is found to redevelop a boundary-layer-like region near the surface. The effects of this boundary-layer-like region on the flowfield and heating rates are discussed.

Nomenclature

H = nondimensional total enthalpy, $\bar{H}/\bar{V}_\infty^2$
h = nondimensional specific enthalpy, $\bar{h}/\bar{V}_\infty^2$
M_∞ = freestream Mach number
$\dot{m}$ = surface blowing rate, $\bar{\rho}\bar{v}/\bar{\rho}_\infty\bar{V}_\infty$
$\dot{m}_0$ = surface blowing rate at the axis of symmetry
n = coordinate normal to the body, $\bar{n}/\bar{\rho}_\infty\bar{V}_\infty^2$
p = nondimensional pressure, $\bar{p}/\bar{\rho}_\infty\bar{V}_\infty^2$
R = gas constant, J/kg K
Re = freestream Reynolds number, $\bar{\rho}_\infty\bar{V}_\infty\bar{R}_N/\bar{\mu}_\infty$
$\bar{R}_N$ = nose radius, m
r = body radius normal to the body axis, $\bar{r}/\bar{R}_N$
s = coordinate measured along the body, $\bar{s}/\bar{R}_N$
T = nondimensional temperature, $\bar{T}/\bar{T}_\infty$
$\bar{T}_\infty$ = freestream temperature, K
t = nondimensional time, $\bar{t}\bar{V}_\infty/\bar{R}_N$
u = nondimensional tangential velocity, $\bar{u}/\bar{V}_\infty$
$\bar{V}_\infty$ = freestream velocity, m/s
v = nondimensional normal velocity, $\bar{v}/\bar{V}_\infty$
β = $r+n\cos\theta$
γ = ratio of specific heats
δ = shock standoff distance, $\bar{\delta}/\bar{R}_N$
θ = body angle measured from the body axis
σ = Prandtl number
σ_T = turbulent Prandtl number
λ = $1+n\kappa$
κ = local curvature, $\bar{\kappa}\bar{R}_N$
ρ = nondimensional density, $\bar{\rho}/\bar{\rho}_\infty$
$\bar{\rho}_\infty$ = freestream density, kg/m^3
μ = nondimensional viscosity, $\bar{\mu}/\bar{\mu}_\infty$
μ_T = nondimensional eddy viscosity, $\bar{\mu}_T/\bar{\mu}_\infty$
$\bar{\mu}_\infty$ = freestream viscosity, N s/m^2
ϵ_T = normalized eddy viscosity, μ_T/μ

Superscript

$(\bar{\ })$ = dimensional quantities

Subscripts

w = conditions at the body surface
∞ = conditions in the freestream

Received Feb. 1, 1979; revision received June 7, 1979.

Index categories: Supersonic and Hypersonic Flow; Viscous Nonboundary-Layer Flows.

*Research Associate Professor, Dept. of Mechanical Engineering and Mechanics. Member AIAA.

†Research Leader, Aerothermodynamics Branch, Space Systems Division. Member AIAA.

‡Professor, Dept. of Mechanical Engineering and Mechanics. Member AIAA.

Introduction

THE exploration of the outer planets requires the development of a realistic aerothermal environment to be encountered by the entry probe. The aerothermal environment is characterized by high energy flow, large heat-transfer rates to the probe's surface, and high rate of mass injection from the probe's ablative heat shield into the flow. This requires the development of computer codes that can provide coupled solutions for chemically reacting and radiating flow with massive ablation rates. Most of the solutions available in the literature which include surface blowing are based on the flow over analytical bodies such as hyperboloid.[1-3] These computer codes find difficulty in treating the realistic entry probe shape, viz, the spherically blunted cone with surface blowing. Reference 4 presents some results with surface blowing on spherically blunted cones for air, but the blowing rates considered are very low and the blowing rate distribution is such that it starts at the stagnation point and goes to zero at the sphere-cone juncture point. There is no blowing on the conical part of the body.

The purpose of this paper is to present the solutions for the flow over a spherically blunted cone with massive surface blowing rates. Time-dependent viscous shock layer equations are used to describe the flowfield. The boundary conditions on the body surface include a prescribed blowing rate distribution. The same gas is injected from the surface as is in

the main flowfield. The governing equations are solved by a time-asymptotic finite-difference method. Results presented here are for a perfect-gas-type flow at zero angle of attack and do not include radiative heating or chemical reactions in the flowfield. Both laminar and turbulent solutions are obtained and the effects of massive surface blowing on the flowfield quantities are discussed in detail.

Analysis

The basic equations are obtained from the unsteady Navier-Stokes equations by keeping terms up to second order in the inverse square root of Reynolds number in both the viscous and inviscid regions. A body oriented coordinate system is used in the analysis (see Fig. 1). These time-dependent viscous shock layer equations, developed in Ref. 5, are modified to include the turbulence and are used here to describe the flowfield. The present analysis is for a perfect gas flow at zero angle of attack and does not include radiative heating or chemical reactions in the flowfield.

Governing Equations

The governing equations are expressed in the nondimensional conservative form as

$$\frac{\partial U}{\partial t}+\frac{\partial M}{\partial s}+\frac{\partial N}{\partial n}+Q=0 \tag{1}$$

where

$$U=\lambda\begin{bmatrix}\rho\\ \rho u\\ \rho v\\ \rho H-p\end{bmatrix},\qquad M=\begin{bmatrix}\rho u\\ \rho u^2+p\\ \rho uv\\ \rho uH\end{bmatrix},\qquad N=\lambda\begin{bmatrix}\rho v\\ \rho uv-\dfrac{\mu}{Re}(1+\epsilon^+)\dfrac{\partial u}{\partial n}+\dfrac{\mu u\kappa}{\lambda Re}\\ p+\rho v^2\\ \rho vH-\dfrac{\mu}{\sigma Re}\left(1+\epsilon^+\dfrac{\sigma}{\sigma_T}\right)\dfrac{\partial h}{\partial n}-\dfrac{\mu u}{Re}(1+\epsilon^+)\dfrac{\partial u}{\partial n}+\dfrac{\mu u^2\kappa}{\lambda Re}\end{bmatrix}$$

$$Q=\frac{\lambda\sin\theta}{\beta}M+\frac{\cos\theta}{\beta}N+\frac{1}{\beta}\begin{bmatrix}0\\ \beta\kappa\rho uv-\dfrac{\mu}{Re}(1+\epsilon^+)\beta\kappa\dfrac{\partial u}{\partial n}-p\lambda\sin\theta+\dfrac{\mu u\beta\kappa^2}{\lambda Re}\\ -\beta\kappa\rho u^2-p(\lambda\cos\theta+\beta\kappa)\\ 0\end{bmatrix}$$

These equations are not valid at the axis of symmetry. A limiting form of the governing equations is obtained by differentiating Eq. (1) with respect to s and taking the limit as $s\to 0$. The following equations are obtained at the axis of symmetry.

$$\frac{\partial U_0}{\partial t}+\frac{\partial M_0}{\partial s}+\frac{\partial N_0}{\partial n}+Q_0=0 \tag{2}$$

where

$$U_0=\lambda\begin{bmatrix}\rho\\ \rho u\\ \rho v\\ \rho H-p\end{bmatrix},\qquad M_0=\begin{bmatrix}2\rho u\\ p+2\rho u^2\\ 2\rho uv\\ 2\rho uH\end{bmatrix},\qquad N_0=\lambda\begin{bmatrix}\rho v\\ \rho uv-\dfrac{\mu}{Re}\left(\dfrac{\partial u}{\partial n}-\dfrac{\mu\kappa}{\lambda}\right)-\dfrac{\mu\epsilon^+}{Re}\dfrac{\partial u}{\partial n}\\ p+\rho v^2\\ \rho vH-\dfrac{\mu}{\sigma Re}\dfrac{\partial h}{\partial n}+\dfrac{\mu\epsilon^+}{\sigma_T Re}\dfrac{\partial h}{\partial n}-\dfrac{\mu u}{Re}\left(\dfrac{\partial u}{\partial n}-\dfrac{u\kappa}{\lambda}\right)-\dfrac{\mu\epsilon^+}{Re}u\dfrac{\partial u}{\partial n}\end{bmatrix}$$

$$Q_0=\kappa\begin{bmatrix}\rho v\\ 2\left\{\rho uv-\dfrac{\mu}{Re}\left(\dfrac{\partial u}{\partial n}-\dfrac{u\kappa}{\lambda}\right)-\dfrac{\mu\epsilon^+}{Re}\dfrac{\partial u}{\partial n}\right\}\\ \rho(v^2-u^2)-p\\ \rho vH-\dfrac{\mu}{\sigma Re}\dfrac{\partial h}{\partial n}-\dfrac{\mu\epsilon^+}{\sigma_T Re}\dfrac{\partial h}{\partial n}-\dfrac{\mu u}{Re}\left(\dfrac{\partial u}{\partial n}-\dfrac{u\kappa}{\lambda}\right)-\dfrac{\mu\epsilon^+}{Re}u\dfrac{\partial u}{\partial n}\end{bmatrix}$$

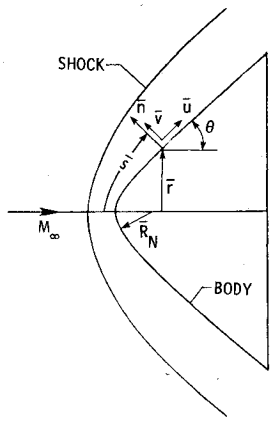

Fig. 1 Coordinate system.

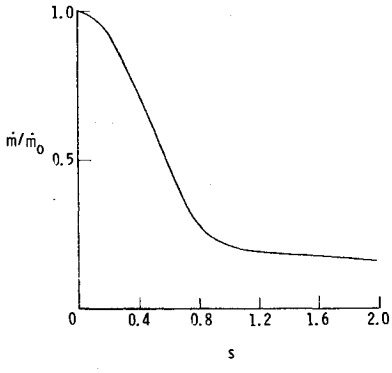

Fig. 2 Surface blowing rate distribution.

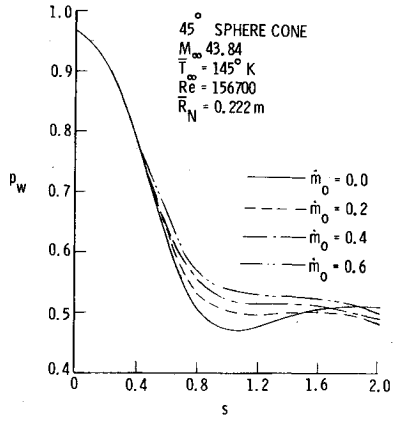

Fig. 3 Surface pressure distribution with surface blowing.

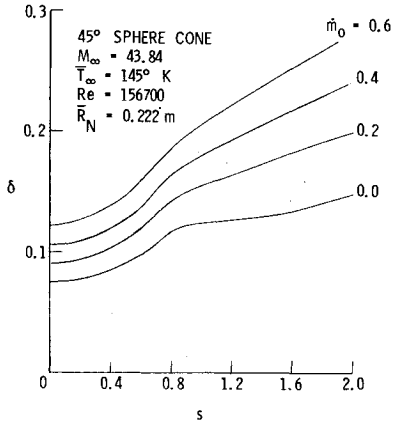

Fig. 4 Shock standoff distances with surface blowing.

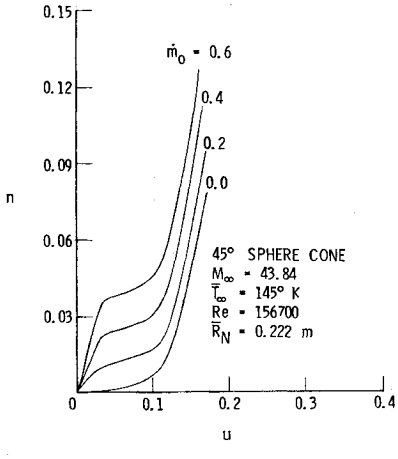

Fig. 5 Tangential velocity profile variation with surface blowing at $s=0.196$.

In addition to the above equations, an equation of state and a viscosity law are used to complete the set of governing equations. These are given below:

$$p=(\gamma-1)\rho h/\gamma \tag{3}$$

$$\mu=T^{0.65} \tag{4}$$

Boundary Conditions

Along the body surface, no-slip boundary conditions are used. The wall temperature is taken as a specified value. A prescribed surface blowing rate distribution is used. For the Jovian entry probe, a typical surface blowing rate distribution is shown in Fig. 2 which is used in the present investigation.

The shock is treated as a sharp discontinuity and shock relations are used to calculate the flow conditions immediately behind the shock. The flow quantities along the supersonic outflow boundary are determined by extrapolation from the inner mesh points.

Eddy Viscosity Approximation

A two-layer eddy viscosity model consisting of an inner law based upon Prandtl's mixing length concept and the Clauser-Klebanoff expression (based on Refs. 6 and 7) for the outer law is used in the present analysis. This model, introduced by Cebeci,[8] assumes that the inner law is applicable for the flow from the wall out to the location where the eddy viscosity given by the inner law is equal to that of the outer law. The outer law is then assumed applicable for the remainder of the viscous layer. Reference 2 gives a detailed description of the eddy-viscosity model. In the present investigation, the turbulent Prandtl number is set equal to 0.9.

Method of Solution

The numerical solutions are obtained in the region bounded by the body and the shock. The shock is treated as a sharp discontinuity across which shock relations are used to compute the flow quantities behind the shock. Two independent variable transformations are applied to the governing equations. The first transformation maps the computational domain into a rectangular region in which both the shock and the body are made boundary mesh lines. The second transformation further maps the computational region into another plane to allow higher resolution near the body surface without too much increase in the number of mesh points in the normal direction.

MacCormack's two-step finite-difference method[9] is used to solve the governing equations. The explicit method has second-order accuracy in both space and time and is highly efficient on a CDC-STAR-100 computer. Since only the steady-state solution is of interest in the present investigation, the solution is marched in time on each mesh point according to its largest possible Courant-Friedrich-Lewy (CFL) time-step size. It is shown in Ref. 10 that the use of local time-step results in a speed up of two or more over the regular Mac-

Cormack scheme in which the solution is marched with global minimum CFL time-step on all of the mesh points. Because of the aforementioned advantages, the present analysis still used the original MacCormack scheme, although several more recent versions are available. The details of the coordinate transformations and the method of solution are given in Ref. 5.

Discussion of Results

Flowfield results are presented for the forebody of the spherically blunted cone with massive surface blowing. Solutions are obtained for both laminar and turbulent flows. The freestream conditions and other parameters used in the analysis are given below:

Gas—hydrogen-helium mixture (under perfect gas assumption)

$M_\infty = 43.84$ $\gamma = 1.224$
$\bar{T}_\infty = 145$ K $R = 3593.6$ J/kg K
$\bar{\rho}_\infty = 1.27 \times 10^{-4}$ kg/m^3 $Re = 156{,}700$
$\bar{R}_N = 0.222$ m $\sigma = 0.72$
$\bar{T}_w = 4000$ K $\bar{\mu} = 2.48 \times 10^{-7} \bar{T}^{0.65}$ Ns/m^2

These conditions correspond to typical Jovian entry conditions.

Laminar Flow

Results of the laminar flow are discussed first. Figure 3 shows the surface pressure distribution over a 45-deg half-angle sphere-cone with increasing surface blowing. It is seen from this figure that, for zero blowing, there is a positive pressure gradient on the conical portion of the body due to the curvature discontinuity at the juncture point. As the blowing rate increases, the positive pressure gradient is reduced, and for $\dot{m}_0 = 0.4$ and higher, the pressure gradient becomes negative. Thus, the surface blowing smooths out the effect of curvature discontinuity at the juncture point on the flowfield and results in a negative pressure gradient all over the body.

Shock standoff distances are shown in Fig. 4. This figure also shows the smoothing out of the curvature discontinuity effects with increasing blowing. It is also seen that the shock standoff distances increase with increasing blowing rate and the shock slope becomes steeper as the blowing rate is increased. It did not create any problems for the present conditions and the body shape, but the flow can become subsonic behind the shock at downstream points of large angle bodies, which will not allow the extrapolation used at the outflow boundary.

Figures 5-7 show the profiles for tangential velocity, enthalpy, and normal velocity at $s = 0.196$, which is located close to the stagnation point on the spherical portion of the body. Figures 5 and 6 show the typical behavior of the shock layer in the presence of surface blowing. It is characterized by an inner inviscid layer, a thin shear layer, and an outer inviscid layer. The extent of the inner layer increases with increasing blowing rates. In the case of an ablating surface, this inner inviscid layer will mainly be containing the ablation gas products.

The normal velocity profiles in Fig. 7 show that the normal velocity decreases slightly in the inner inviscid layer, increases in the shear layer, and then decreases monotonically to the shock value in the outer inviscid layer. The increase in the normal velocity in the shear layer would enhance the mixing of the inner and outer layer gases, thus increasing the thickness of the ablation gas layer. This increase in the ablation layer thickness is particularly important, since most of the attenuation of the radiation takes place in this region.

Tangential velocity, enthalpy, and normal velocity profiles are also plotted at $s = 1.767$, which is located on the conical portion of the body far downstream of the sphere cone juncture point. These are shown in Figs. 8-10. It is seen from

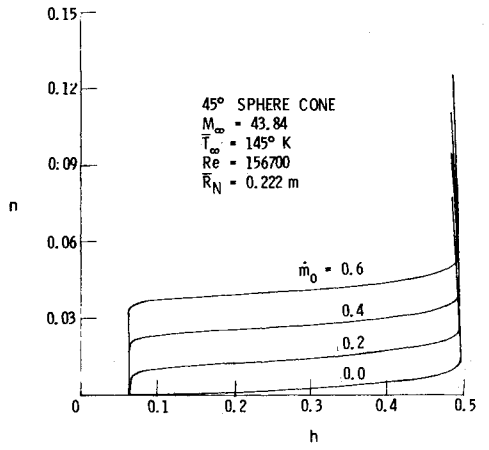

Fig. 6 Enthalpy profile variation with surface blowing at $s = 0.196$.

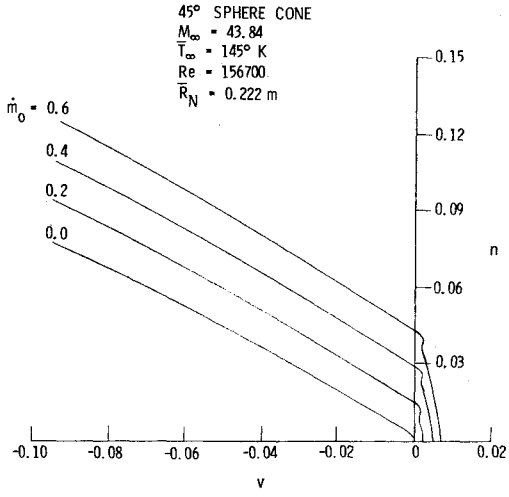

Fig. 7 Normal velocity profile variation with surface blowing at $s = 0.196$.

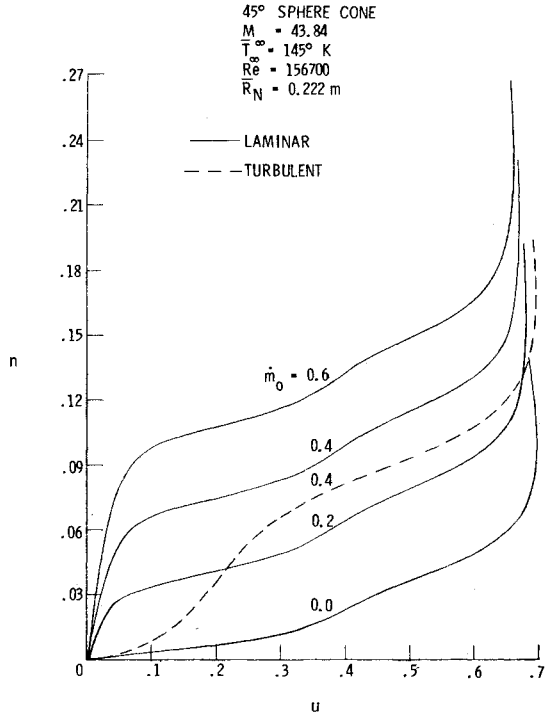

Fig. 8 Tangential velocity profile variation with surface blowing at $s = 1.767$.

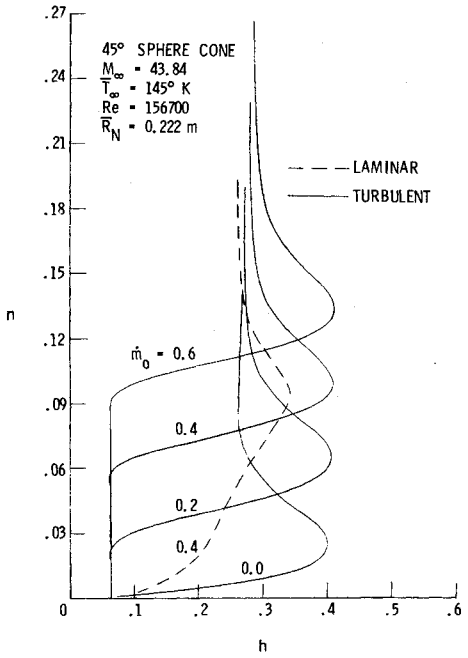

Fig. 9 Enthalpy profile variation with surface blowing at $s = 1.767$.

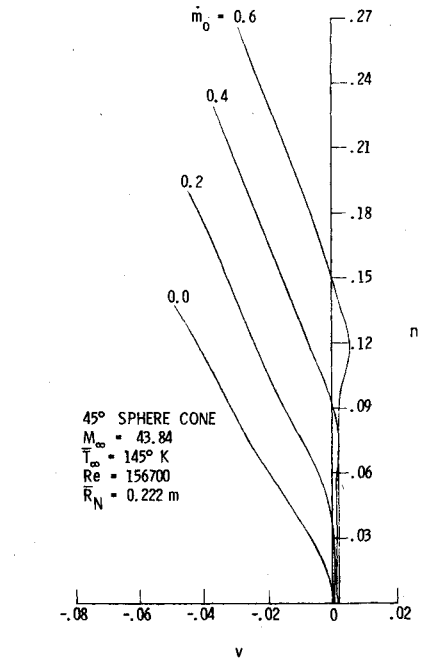

Fig. 10 Normal velocity profile variation with surface blowing at $s = 1.767$.

Fig. 9 that the enthalpy changes rapidly in the inner portion of the outer inviscid layer. This rapid change in the enthalpy forms an entropy layer that was not present in the forward portion of the body. Thus, on the downstream part of the body, the shock layer consists of an inner inviscid layer, a thin shear layer, an entropy layer, and an outer inviscid layer.

Turbulent Flow

For the turbulent solutions, an instantaneous transition is assumed close to the stagnation point at $s = 0.196$. Figure 11 shows a comparison of the surface pressure distribution for the laminar and turbulent flows. For zero blowing, the surface pressures are almost identical in the laminar and turbulent flows. For $\dot{m}_0 = 0.4$, the laminar flow shows a negative pressure gradient whereas the turbulent flow

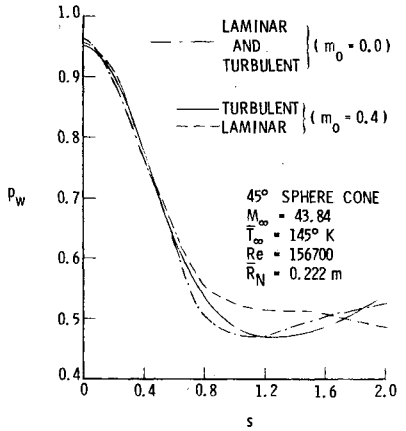

Fig. 11 Surface pressure distribution for laminar and turbulent flows with surface blowing.

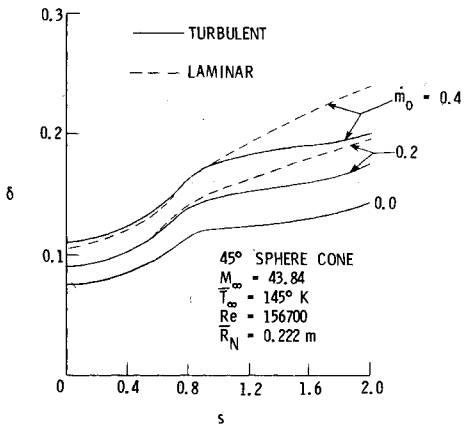

Fig. 12 Shock standoff distances for laminar and turbulent flows with surface blowing.

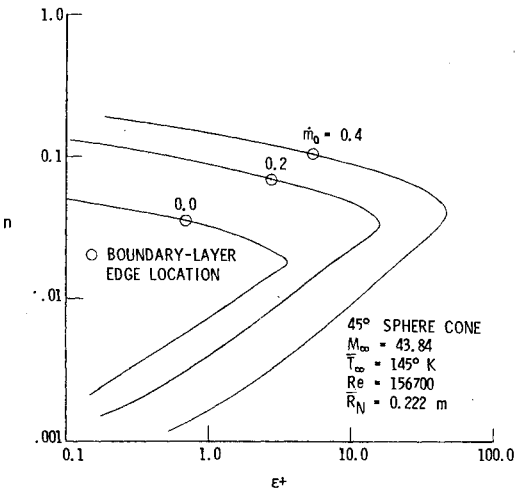

Fig. 13 Eddy viscosity profile variation with surface blowing at $s = 1.767$.

develops again a positive pressure gradient similiar to that for zero blowing.

Figure 12 shows the comparison of shock standoff distances for the laminar and turbulent flows. Here again, the shock standoff distances for the laminar and turbulent flows are almost identical for zero blowing. For nonzero blowing, there is a significant decrease in the shock standoff distances for the turbulent flow at downstream points, thus making the shock relatively less stronger compared to the corresponding

laminar flow. Moreover, the shock slope for the turbulent flow is not seen to increase with increasing blowing rates. The figure shows that for the turbulent flow, the shock is pushed away from the body in the presence of blowing but the shock shape remains similar to that for zero blowing. The reduction in the shock standoff distances can be explained from Fig. 8 in which the turbulent tangential velocity profile for $\dot{m}_0 = 0.4$ is plotted along with the laminar profiles. The magnitude of the tangential velocity is higher all across the shock layer for the turbulent flow, which results in the reduction of the shock standoff distances.

The turbulent tangential velocity profile in Fig. 8 shows that the gradients near the surface are increased significantly due to the turbulent mixing of the flow in the shear layer. Similar increased gradients are also seen in Fig. 9 for the turbulent enthalpy profile. Thus, the turbulent flow with surface blowing redevelops a boundary-layer-like region near the surface. The increased gradients near the surface make the convective heating and skin friction significant for the turbulent flow even in the presence of massive surface blowing whereas these are negligibly small for the corresponding laminar flow. The turbulent enthalpy profile in Fig. 9 also shows that the gradients in the entropy layer are reduced because, for the nonzero blowing, the shock is weaker for the turbulent flow than that for the laminar flow as discussed earlier.

Figure 13 shows the eddy viscosity distribution across the shock layer at $s = 1.767$ for $\dot{m}_0 = 0$, 0.2 and 0.4. It is seen from this figure that the eddy viscosity increases sharply with the increased surface blowing. The two-layer model provides good approximation of the eddy viscosity for zero and small blowing rates but its validity for massive surface blowing rates is not known.

Conclusions

Numerical solutions for the laminar and turbulent flows over a spherically blunted cone are presented with massive surface blowing. It is found that the surface blowing smooths out the effect of curvature discontinuity at the sphere-cone juncture point on the laminar flowfield and results in a negative pressure gradient over the body. The shock slope increases at the downstream points with increasing surface blowing which can create problems by making the flow subsonic behind the shock at downstream points of large angle bodies for certain freestream conditions. The turbulent flow with surface blowing is found to redevelop a boundary-layer-like region near the surface. The increased gradients near the surface in this boundary-layer-like region make the convective heating and skin friction significant even with massive blowing whereas these quantities are negligibly small for the corresponding laminar flow. The shock standoff distances are significantly reduced over the downstream part of the body, which make the shock relatively less strong for the turbulent flow than for the laminar flow.

Results presented here were for the perfect gas-type flow and did not include the radiative heating or chemical reactions in the flowfield. The main purpose of this paper was to study the important features of the flowfield in the presence of massive surface blowing and to demonstrate the capability of the present computer code in providing the solutions for the flow over realistic probe shape with massive surface blowing.

References

[1] Moss, J. N., "Radiative Viscous Shock Layer Solutions with Coupled Ablation Injection," *AIAA Journal*, Vol. 14, Sept. 1976, pp. 1311-1317.

[2] Moss, J. N., Anderson, E. C., and Simmonds, A. L., "The Impact of Turbulence on a Radiating Shock Layer with Coupled Ablation Injection," AIAA Paper 78-1186, Seattle, Wash., July 1978.

[3] Graves, R. A., Jr., "Solutions to the Navier-Stokes Equations for Supersonic Flow over Blunt Bodies with Massive Blowing," Ph.D. Dissertation, George Washington University, Washington, D.C., Nov. 1977.

[4] Gogineni, P. R., Murray, A. L., and Lewis, C. L., "Viscous Flows Over Slender Spherically Blunted Cones at Large Angle of Attack Including Mass-Transfer and Low Reynolds Effects," AIAA Paper 78-1188, Seattle, Wash., July 1978.

[5] Kumar, A. and Graves, R.A., Jr., "Numerical Solutions of the Viscous Hypersonic Flow past Blunted Cones at Angles of Attack," *AIAA Journal*, Vol. 15, Aug. 1977, pp. 1061-1062.

[6] Clauser, F. H., "The Turbulent Boundary Layer," *Advances in Applied Mathematics*, Vol. 4, edited by H. L. Dryden and Th. Von Karman, Academic Press, New York, 1956, pp. 1-51.

[7] Klebanoff, P. S., "Characteristics of Turbulence in a Boundary Layer with Zero Pressure Gradient," NACA Rept. 1247, 1955.

[8] Cebeci, T., "Behavior of Turbulent Flow near a Porous Wall with Pressure Gradient," *AIAA Journal*, Vol. 8, Dec. 1970, pp. 2152-2156.

[9] MacCormack, R. W., "The Effect of Viscosity in Hypervelocity Impact Cratering," AIAA Paper 69-354, Cincinnati, Ohio, April 1969.

[10] Kumar, A. and Graves, R. A., Jr., "Comparative Study of the Convergence Rates of Two Numerical Techniques," *AIAA Journal*, Vol. 16, Nov. 1978, pp. 1214-1216.